Scanned-probe detection of electron spin resonance from a nitroxide spin probe
SUPPORTING INFORMATION

Eric W. Moore,[1] SangGap Lee,[1] Steven Hickman,[1] Sarah Wright,[1]
Lee E. Harrell,[2] Peter Borbat,[1] Jack Freed,[1] and John A. Marohn[1,*]

[1]*Department of Chemistry and Chemical Biology*
Cornell University, Ithaca, New York 14853-1301

[2]*Department of Physics*
U.S. Military Academy, West Point, New York 10996

(Dated: April 24, 2009)

I. SAMPLE PREPARATION

The sample was prepared by dissolving 0.0063 g of TEMPAMINE (4-amino-2,2,6,6-tetramethylpiperidine-1-oxyl; Aldrich, 163945) in 1 mL of d_8-toluene, 0.33 mL of which was further diluted to 1 mL and from that, a 0.1 mL alliquot was added to a solution of 0.039 g deuterated polystyrene (Polymer Source, P4179B-dPS, $M_n = 200 \times 10^3$ and $M_w/M_n = 1.4$) in 0.9 mL of d_8-toluene. The resulting solution was spun at 2000 rpm for 30 s onto a 250 μm thick quartz chip (NOVA Electronics). Film thickness was determined by profilometry. A top coating of 20 nm of gold was electron-beam evaporated onto the chip at a rate of 0.2 nm/s. Samples for characterization by low temperature pulsed ESR were prepared identically, minus the gold, removed from the substrate and inserted into a 2 mm o.d. Suprasil tube.

II. PROBE AND NANOPOSITIONING

All experiments were carried out in a custom-built probe operating at $T = 4.2$ K and $P \leq 10^{-6}$ mbar. A thermistor measured temperature near the sample; with microwaves applied, we observed $T \sim 8$ K at this thermistor. Coarse and fine tip-sample positioning was carried out using a commercial nanopositioner (Attocube Systems AG, ANPx51/HV/LT) onto which the cantilever assembly was mounted. The initial surface approach was monitored by applying 8V to the gold coating on the sample and watching the cantilever frequency as the nanopositioner was stepped. The sample location was determined unambiguously by gently touching the cantilever to the sample surface by extending the nanopositioner's piezo with a DC voltage. After the surface was located, all subsequent tip-sample changes were carried out by adjusting this DC voltage. A 1310 nm fiber interferometer was used to calibrate the piezo in situ. The piezo extension was typically found to be 9 nm/V at 8 K.

III. SIMULATION DETAILS

The sample was simulated as a 27 μm $\times$ 24 μm $\times$ 0.215 μm box represented as a grid of 1390 $\times$ 1390 $\times$ 10 points. The tip was modeled as a uniformly magnetized sphere. The magnetic field and its second derivative G' were calculated at each grid point. The z component of spin magnetization was simulated using the Bloch equations, with measured T_1, T_2, B_1, and calculated spin density as inputs. The Curie-law magnetic moment per spin was taken to be 3.59×10^{-25} J/T-spin (for $B_0 = 0.632$ T and $T = 11$ K) and the spin density taken to be 2.41×10^{25} spins/m^3 (appropriate for a 40 mM TEMPAMINE sample). A magnetization profile was computed with the cantilever at its maximum extension; this profile was translated in the x direction to mimic the cantilever oscillation, and the smallest z-magnetization at each grid point retained to mimic the saturated slice. To calculate the spring constant shift, the resulting magnetization profile was multiplied by the volume and second derivative at each point and summed over the entire sample. The temperature (e.g., Curie-Law magnetization) was varied to give good agreement between simulation and experiment.

In the manuscript we reported that spins in the slice at field B_c in Fig. 3 see a G' as large as 8.5×10^{10} T/m^2. As a check, let us compute G' for spins analytically. This calculation is only easily done for spins directly below the tip. In the spin modulation scheme of Fig. 2 in the manuscript spins directly below the tip are not modulated and therefore do not contribute to signal. Nevertheless, spins in the slice at field B_c are not far off axis and so this analytical result will be approximately correct. Modeling the tip as a uniformly magnetized sphere, the field gradient is $G' = \mu_0 M_{\text{tip}} r_{\text{tip}}^{-2}(1 + h/r_{\text{tip}})^{-5}$ at a distance h below the tip. Taking $h = 120$ nm and using measured tip parameters, we estimate $G' = 9.3 \times 10^{10}$ T/m^2, in good agreement with the maximum field second derivative 8.5×10^{10} T/m^2 seen by spins in the B_c slice in the numerical simulation.

*Email:jam99@cornell.edu

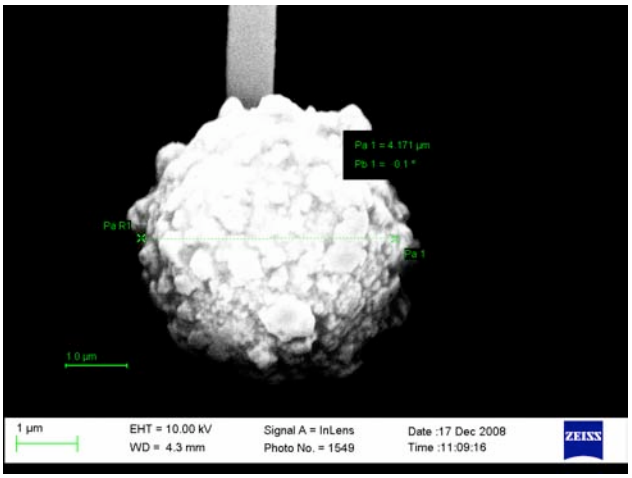

FIG. 1: Scanning electron micrograph of the cantilever's nickel tip.

IV. CANTILEVER FABRICATION AND CHARACTERIZATION

The silicon cantilever (200μm long, 4μm wide, and 0.34μm thick) was fabricated as detailed in Jenkins et al. [1]. The last 5 μm of the cantilever is only 1 μm wide. The magnet was attached to this narrow section as follows. A small amount of magnetic powder (Novamet, CNS-10, nominal diameter 4μm) was dispersed onto a surface. While observing through an inspection microscope, optical micrometer stages were used to touch the cantilever tip to a small drop of epoxy (Miller-Stephenson 907) and then to an isolated magnetic particle. The anisotropy of these particles is small enough that allowing the epoxy to cure in an applied field to align the magnetic easy-axis with the field direction [2] was not necessary. A scanning electron micrograph of the magnetic particle affixed to the cantilever end can be seen in Fig. 1.

Cantilever motion was detected using a temperature-tuned [3] optical-fiber interferometer [4] (wavelength 1310 nm; cantilever-incident power $\sim 3\mu$W) and a New Focus Model 2011 photodetector. The interferometer's optical fiber was aimed at a reflective pad (octagonal, 30 μm side-to-side) fabricated 75 μm from the cantilever end. Modeling the tip as a singly clamped beam of rectangular cross section, we estimated that the tip deflection is 2.02 times larger at the cantilever end than at the reflective pad [5]. The cantilever's spring constant was determined by observing thermomechanical flutuations in position at the reflective pad, multiplying the observed signal by 2.02 to get the thermomechanical fluctuations at the tip $x_{\rm th}$, and calculating the spring constant from $k = k_B T/\langle x_{\rm th}^2\rangle$. The cantilever's quality factor was calculated from the measured $1/e$ ringdown time τ using $Q = \pi f_0 \tau$. The Q was identical if measured on a positive-going or negative-going interferometric fringe, indicating that the observed Q is not being reduced or enhanced by optical-pressure feedback [6].

V. CANTILEVER FREQUENCY MEASUREMENT AND MICROWAVE SYNCHRONIZATION

To measure cantilever frequency, the cantilever was driven into self oscillation [7] and the digitized oscillation fed into a software frequency demodulator [8]. To achieve self-oscillation, the cantilever signal was passed through a custom-built cantilever controller and fed back into a piezoactuator at the cantilever base. In the custom-built cantilever controller the input signal was filtered using a $Q = 0.625$ pass-band filter centered at the cantilever's resonance frequency, phase shifted by $-90°$, converted to a 5 V peak-to-peak square wave using a comparator, multiplied with a set DC voltage to reach a full-fringe amplitude, and then filtered using a $Q = 2.5$ pass-band filter centered at the cantilever's resonance frequency. The key feature of the circuit was that it was equipped with a flat-gain large-range phase shifter and an automatic gain controller (a voltage comparator followed by a band pass filter).

For the frequency shift protocol of Fig. 2 the frequency of the square-wave copy of the cantilever oscillation was digitally divided down using 12-bit binary counters to produce a square wave at $f_{\rm mod}$ and a square wave at the pulse repetition rate, both synchronized to the canitlever oscillation. These two waves were AND-gated together and the output used to trigger a pulse/delay generator (Berkeley Nucleonics, model 565). This system can maintain cantilever synchronization over long times. The phase-based T_1 measurements used a single cantilever based trigger to produce the burst of 32 pulses. The output of the pulse/delay generator was sent to the microwave switch.

VI. MICROWAVE DELIVERY AND PERFORMANCE

Microwaves were supplied by an Anritsu-Wiltron source (model 68147B), routed through a switch (American Microwave Corporation, model SWN-218-2DT, options 912 and B05HS20NS) and an amplifier (Nardamicrowave, model DBP-0618N830). The peak power out of the amplifier was approximately 32.5 dBm. This power was attenuated by 8.5 dBm by the 4.5 m of cable leading to the resonator. The power reported in the saturation experiment is the estimated power delivered to the stripline resonator.

The resonator depicted in Fig. 1 of the manuscript was fabricated on a commercially available printed circuit board. The copper resonator was 5.6 mm long, 1.4 mm wide, and 36 μm thick; the epoxy-glass dielectric was 0.7 mm thick; and the coupling gap was $20 - 40$ μm wide. The electrical quality factor of the resonator itself was ~ 800, as determined by a lock-in reflectance measurement using a directional coupler (Krytar Model 102020020) and an RF power detector (Anritsu-Wiltron Model 75KA50). To characterize electrical resonances in situ, we amplitude-modulated the microwaves at f_0 using a switch and observed the resulting cantilever excitation using a lock-in amplifier with the cantilever located tens

of microns from the sample surface. We identified three resonances in situ: 9.82, 13.79, and 17.99 GHz. The last resonance shifted to 17.73 GHz on cool down.

Let us estimate the how much larger a B_1 would be required to carry out a high-efficiency adiabatic rapid passage. To achieve a high-efficiency rapid passage, the adiabaticity parameter, $c_a = \gamma B_1^2 (dB_{\text{eff}}/dt)^{-1}$, should be $\gg 1$. Here $dB_{\text{eff}}/dt = dB_{\text{tip}}/dx \times dx/dt$. For simplicity consider a spherical tip of radius r_{tip} operating at height $h = 0$. Surface spins at location $x = r_{\text{tip}}/2$ will see the largest gradient, $G \approx 0.29\mu_0 M_{\text{tip}}$. For a sinusoidally-driven cantilever, $x(t) = x_{0\text{p}} \cos(2\pi f_0 t)$, and we estimate

$$c_a \approx \frac{0.55\gamma B_1^2 r_{\text{tip}}}{\mu_0 M_{\text{tip}} f_0 x_{0\text{p}}}. \quad (1)$$

For $x_{0\text{p}} = 163$ nm, $r_{\text{tip}} = 1.85$ μm, $B_1 = 3.9$ mG, $\mu_0 M_{\text{tip}} = 0.44$ T, and $f_0 = 5$ kHz, we estimate $c_a = 6.5 \times 10^{-6}$. A field of amplitude $B_1 \geq 1.5$ G would be required to achieve $c_a \geq 1$ in our experiment.

VII. CANTILEVER FREQUENCY NOISE

The frequency noise experienced by the cantilever was investigated at a series of tip-sample heights. While the cantilever was self-oscillated as described above, the cantilever position was recorded for 25 second intervals and the instananeous frequency calculated. Power spectra were computed from these frequency traces; $n_{\text{avg}} = 25$ power spectra were averaged together to give the spectra ploted in Fig. 2. At the largest tip-sample heights the low frequency cantilever frequency fluctuations have the expected magnitude, given the mechanical properties of the cantilever and the temperature (here $T = 4.2$ K). As the cantilever is approached toward the surface, low frequency surface induced frequency fluctuations begin to grow in. At the closest tip-sample spacings used, the surface induced frequency noise sets the noise floor for our measurement.

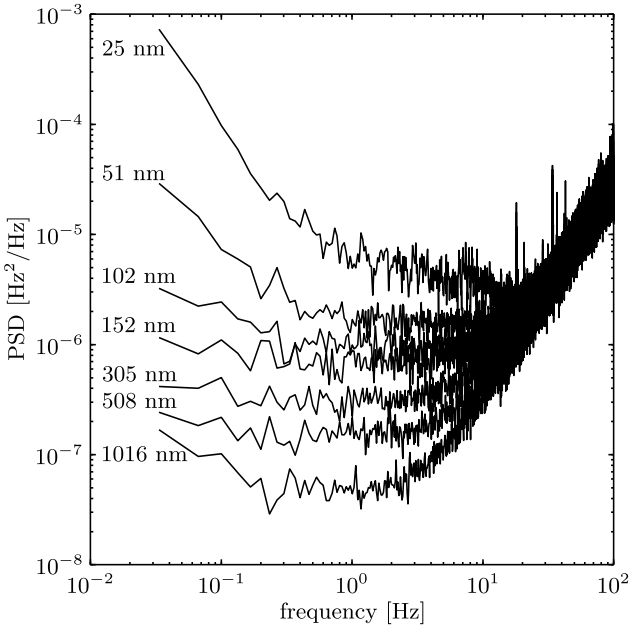

FIG. 2: Cantilever frequency power spectra for a series of tip-sample heights. At high frequencies the power spectra are dominated by detector noise and proportional to f^2. At lower frequencies and large tip-sample heights, the magnitude is set by the mechanical properties and the temperature of the cantilever. At the smallest tip-sample heights, surface induced noise is the dominant source of cantilever frequency noise.

VIII. INDUCTIVELY-DETECTED ESR T_1 AND T_2 MEASUREMENT

Samples were prepared for analysis by inductively detected ESR as described in the main text. A two-pulse primary echo sequence was used to measure T_1 and T_2. Figure 3A is a plot of the primary echo amplitude versus pulse repetition frequency f. The sample T_1 was estimated by fitting the primary echo amplitude V to [9]

$$V(f) = V(0)(1 - e^{-1/(fT_1)}) \quad (2)$$

where $V(0)$ is the echo amplitude, measured at a repetition frequency of a few hertz, and T_1 is the spin-lattice relaxation time. The $\pi/2$ and π pulses, separated by 250 ns, were of duration 16 and 32 ns respectively. At low repetition rates (< 500Hz) the data deviates from a simple exponential dependence, as one would expect for this temperature. A 20% uncertainty in T_1 mostly originates from a small background impurity signal that was present in the resonator at the time of the measurements. The sample T_2 was determined from the primary echo decay, Fig. 3B, using 45/90 ns pulse widths. Instantaneous diffusion was only a very minor effect, due to suppression by a fast spin flip rate, which apparently was a major source of the short relaxation time found.

IX. FREQUENCY BASED T_1 MEASUREMENT

Using a phase-based measurement protocol we found good agreement between sample T_1 measured using MRFM and sample T_1 measured via standard ESR techniques. Prior to these phase based measurements, we attempted to measure the T_1 by following the spin-induced cantilever frequency shift as a function of the time between microwave pulses in the Fig. 2 protocol of the manuscript. We found this approach problematic. At constant f_{mod}, the background signal varied with duty cycle and therefore n, making it difficult to see the expected exponential dependence of spin signal on pulse delay, Eqs. 2 and 3 in the manuscript, on top of the varying background. Varying n but keeping duty cycle constant mitigated this complication, but required either simultaneously varying f_{mod} or

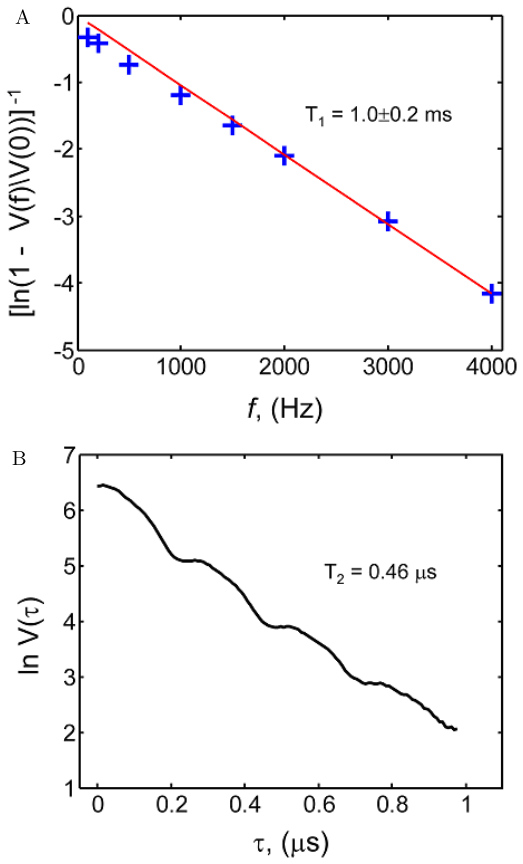

FIG. 3: Relaxation times measurements of TEMPAMINE in perdeuterated polysterene by pulsed ESR at 4.16 K. (A) Primary echo amplitude versus repetition frequency. (B) Primary echo decay.

using pulse sequences with unequal on and off durations, both of which led to data that was not straightforward to interpret.

A representative data set is shown in Fig. 4. This measurement was carried out as indicated in Fig. 2 of the manuscript with the time between pulses stepped by one cantilever cycle between each point while the number of pulses in each on-cycle was held fixed. Because of the low-pass filter present in the software frequency demodulator, the measured signal reflects the low-frequency moduation at $f_{\rm mod}$ and not the high-frequency modulation induced individually by each pulse. When the time between pulses becomes large, the frequency shift seen Fig. 4 in decays, we hypothesize, because the smoothed spin-induced cantilever frequency modulation (Fig. 2F in the manuscript) is no longer well approximated by square wave at $f_{\rm mod}$ (although the spin-induced cantilever frequency shift maintains much of its power at the pulse repetition rate).

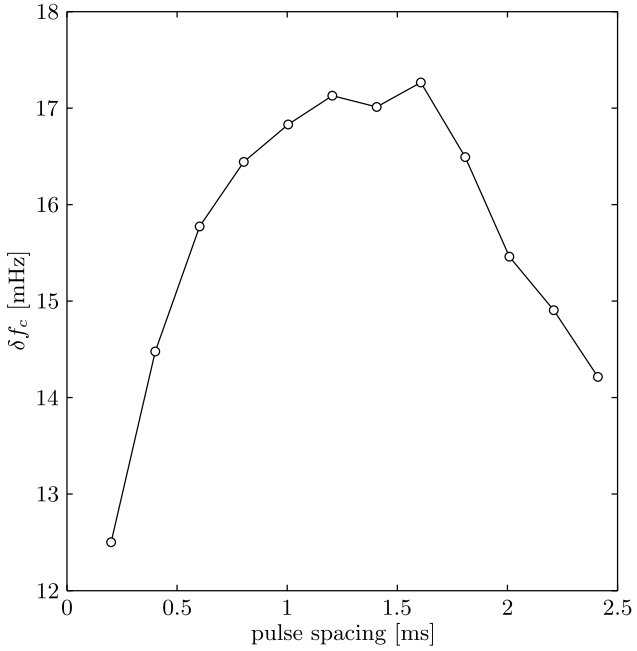

FIG. 4: A representative data set for a frequency shift T_1 measurement. This data is from the peak at field B_b.

X. TEMPAMINE g-FACTOR

While the ESR spectrum of TEMPAMINE cannot be observed directly in our experiment because of inhomogeneous broadening of the resonance by the tip field, we can measure the g factor with enough precision to demonstrate that the signal in our experiment is due to unpaired electrons with $g \sim 2.0$. To do this, we applied the microwaves at two other eigenfrequencies of our halfwave resonator (present, we conjecture, due to nonidealities in the stripline). A plot of the location of the B_b peak versus microwave frequency is shown in Fig. 5. From the slope of the line we infer $g = 2.026 \pm 0.003$. This is in poor agreement with $g = 2.0057$ measured by conventional ESR for TEMPAMINE [10]. The value of g that we measure differs from the accepted value for TEMPAMINE for a number of reasons. The main sources of error are uncertainty in the tip field as the external field is reduced, magnetostriction in the z piezo causing changes in the tip height as the field is changed, a change in tip magnetization during the field ramp, and difficulty extracting the resonance field from the data given the complicated lineshape.

References

[1] Jenkins NE, *et al.* (2004) Batch fabrication and characterization of ultrasensitive cantilevers with submicron magnetic tips. *J Vac Sci Technol B* 22:909–915.

[2] Garner SR, Kuehn S, Dawlaty JM, Jenkins NE, Marohn JA (2004) Force-gradient detected nuclear magnetic resonance. *Appl Phys Lett* 84:5091–5093.

[3] Bruland KJ, *et al.* (1999) Thermal tuning of a fiber-optic interferometer for maximum sensitivity. *Rev Sci Instrum* 70:3542–

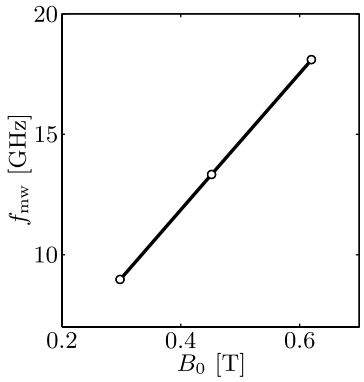

FIG. 5: Plot of microwave frequency, $f_{\rm mw}$, verses the location of the B_b peak. The slope of a line fit to the data is proportional to the g factor for the electrons in the sample. From the fit we extract, $g = 2.026 \pm 0.003$. Microwaves frequencies used were 8.99 GHz, 13.33 GHz, and 18.10 GHz.

3544.

[4] Rugar D, Mamin HJ, Guenther P (1989) Improved fiber-optic interferometer for atomic force microscopy. *Appl Phys Lett* 55:2588–2590.

[5] Sidles JA, *et al.* (1995) Magnetic resonance force microscopy. *Rev Mod Phys* 67:249 – 265.

[6] Kim K, Lee S (2002) Self-oscillation mode induced in an atomic force microscope cantilever. *Appl Phys Lett* 91:4715 – 4719.

[7] Albrecht TR, Grütter P, Horne D, Rugar D (1991) Frequency-modulation detection using high-q cantilevers for enhanced force microscope sensitivity. *J Appl Phys* 69:668 – 673.

[8] Yazdanian SM, Marohn JA, Loring RF (2008) Dielectric fluctuations in force microscopy: Noncontact friction and frequency jitter. *J Chem Phys* 128:224706.

[9] Ernst RR, Bodenhausen G, Wokaun A (1990) *Principles of Nuclear Magnetic Resonance in One and Two Dimensions* (Oxford University Press, USA).

[10] Bajaj VS, *et al.* (2003) Dynamic nuclear polarization at 9 T using a novel 250 GHz gyrotron microwave source. *J Magn Reson* 160:85–90.